

Porous Ceramic Materials From Polysiloxane-Clay Composites

Mariana G. Segatelli,*^{a,b} Manuela L. Q. A. Kaneko,^a Viviane P. Silva^a and Inez V. P. Yoshida^a

^aInstitute of Chemistry, University of Campinas (UNICAMP), 13083-970 Campinas-SP, Brazil

^bDepartment of Chemistry, University of Londrina (UEL), 86057-970 Londrina-PR, Brazil

Este trabalho descreve as alterações estruturais, texturais e morfológicas de cerâmicas porosas derivadas de polímeros e obtidas pela pirólise de compósitos polissiloxano/argila, contendo formador de poros à base de poli(dimetilsiloxano) e acetato de níquel como indutor de nanoestruturas. Os compósitos foram obtidos a partir de molde de aço-inox, seguido por tratamento térmico a 950 °C e 1500 °C (atmosfera inerte). O aumento da temperatura associado com a presença de Ni resultou em cerâmicas mais cristalinas e porosas, além de maior ordenamento da fase de C_{livre}. As cerâmicas revelaram ampla faixa de tamanho de poros. Em 950 °C, foram gerados poros e ilhas ricas em Ni e C dispersas na superfície de fratura. Entretanto, a 1500 °C, foram obtidos nanofios com alta razão de aspecto constituídos de Si, C e O. Assim, a presença de Ni associada a maior quantidade de poros originou um ambiente apropriado para a nucleação e crescimento de nanofios de SiCO.

This study describes the structural, porosity and morphological changes of porous polymer-derived ceramics obtained by pyrolysis of polysiloxane-clay composites, containing a pore former based on poly(dimethylsiloxane) and nickel acetate as nanostructure inductor. The composites were blended in a steel mold, thermally treated at 950 °C and 1500 °C (inert atmosphere). The increase of the temperature together with the presence of Ni resulted in more crystalline and porous ceramics and a higher ordering process of C_{free} phase in the Ni-containing sample. The ceramics revealed a wide pore size distribution, from micro to macropores. At 950 °C the ceramic revealed the presence of pores and Ni- and C-rich islands dispersed on the fracture surface. However, at 1500 °C, nanowires with large aspect ratio, constituted by Si, C and O elements were generated. Thus, the presence of Ni associated to higher pores amount gave rise to an appropriate environment for the nucleation and growth of SiCO nanowires.

Keywords: polysiloxane, ceramic matrix composites, clay, pyrolysis

Introduction

During the last years many studies have been focused on the preparation of silicon oxycarbide ceramics by pyrolysis of polymeric precursors.¹⁻⁴ These materials, also known as polymer-derived ceramics (PDCs), possess the general formula SiC_xO_{4-x} + C, where 0 ≤ x ≤ 4 and C corresponds to the free carbon in the molecular structure, i.e., the secondary phase constituted of carbon atoms that are not bonded in the network. The presence of this phase, which is associated to the incomplete thermal degradation of aliphatic and aromatic hydrocarbons species, under an inert atmosphere, can be controlled by the prior selection of the polymeric precursor. The partial substitution of oxygen

by carbon leads to the production of carbidic carbon units, which increase the bond density and, consequently, the network structure strengthen.⁵ In this way, typical physical and chemical properties, such as the glass transition temperature, elastic modulus, hardness and chemical durability are also expected to increase.

In spite of PDCs present the possibility to be produced by different conventional polymer processing techniques (spinning, warm pressing, injection-molding and blowing, for example), the main drawbacks of these materials are the pronounced shrinkage and formation of cracks in the final material structure, as a consequence of the density increase and gaseous substances release during the polymer-ceramic conversion by pyrolysis route.^{6,7} An alternative of minimizing and/or controlling the shrinkage and generation of cracks in the ceramic materials can be

*e-mail: msegatelli@yahoo.com.br

achieved from the incorporation of suitable fillers (active or inactive) in the polymeric precursor, as first described by Greil,⁸ generating ceramic matrix composites (CMC). Moreover, the addition of fillers has also been carried out to improve the integrity and mechanical properties of final ceramic materials.⁹ Typical active fillers (Ti, Zr, Cr and Mo), under pyrolysis in inert atmosphere, may react with the gaseous decomposition products from polymeric precursor as well as pyrolysis gas, giving rise to secondary phases in the resulting ceramics, mainly consisting of carbides and nitrides. However, inactive fillers (SiC and Si₃N₄, for example) do not react with such decomposition products and, in this case, the total shrinkage can partially be reduced by filler volume effect. The process developed by Greil⁸ and associated with the incorporation of such fillers is called AFCOP (active-filler-controlled polymer pyrolysis).

On the other hand, porous polymer-derived ceramics are considered a promising search field and have attracted much attention of researches due to the wide range of technological applications, such as catalyst supports,¹⁰ separation,¹¹ chemical sensing,¹² and more recently, hydrogen storage.¹³ In fact, porosity for dense or porous SiCO ceramics has a great effect on their applications (mechanical strength, thermal conductivity, adsorption, etc.) and many studies have been reported in order to obtain optimized properties by controlling surface area, amount, structure and pore size distributions.^{1,14,15} Different manufacturing processes of porous polymer-derived ceramics have been proposed, including replica of a polymeric template, direct foaming of a solution, use of sacrificial pore formers, etching of suitable fillers, self-assembly of a preceramic polymer, infiltration into meso-porous template and synthesis of an inorganic-organic diblock copolymer.¹⁶⁻²⁰ All these proposed processing methods have showed to be capable to produce ceramics with engineered porosity affording varied and tailored characteristics, which are of interest for a wide range of applications. In this sense, siloxane-clay composites are attractive ceramic precursors, for which few studies have been done. Taking into account that clays are basically composed by silicate, the introduction of this phase aims to improve the strength of porous ceramic walls. During pyrolysis process, the pressure imposed by the pore formers degradation can induce the opening of clay galleries and release of silicate layers on porous ceramic structure.²¹ In addition, the catalytic activity of the Ni transition metal on the production of ceramic nanophases²² is well known, such as nanowires, nanotubes and nanocables, generating materials with future applications, mainly in the electronic and/or optical fields.²³

The present study reports the synthesis and characterization of porous ceramics derived from polysiloxane-clay composites, containing Ni and poly(dimethylsiloxane-co-methylpropylethylene oxide siloxane) as inductor of nano/microstructures and pore former agent, respectively. The natural clay was employed in order to obtain more straightforward ceramic matrix composites, mainly at walls of porous ceramic. The as-prepared ceramic products pyrolysed under inert atmosphere at 950 °C and submitted to a heat treatment at 1500 °C were investigated in terms of their structural, textural and morphological features. In addition, the effect of Ni on the nano/microstructures formation of porous polymer-derived ceramic composites was evaluated.

Experimental

Starting materials

Natural montmorillonite GEL MAX 400, MT, was supplied by Eduardo Vasconcelos Representações LTDA (Porto Alegre, Brazil). MT is a polycationic clay with cation exchange capacity of 106 mequiv (100 g)⁻¹ and real density of 1.54 g cm⁻³. The elemental composition (wt.%) of the MT clay determined by X-ray fluorescence is: SiO₂ (60.8), Al₂O₃ (27.4), Fe₂O₃ (2.4), TiO₂ (0.4), MgO (2.7), CaO (2.9), K₂O (3.0), others (0.4). Commercially available poly(methylsiloxane), (HSi(CH₃)O)_n, PMS, (molar weight ca. 2000 g mol⁻¹) and poly(dimethylsiloxane-co-methylpropylethylene oxide siloxane), PDMS-PEO, (molar weight ca. 3100 g mol⁻¹) were supplied by Dow Corning (Hortolândia, Brazil). Divinylbenzene (DVB) was purchased from Aldrich Chemical Corporation (Milwaukee, USA) and dichloro-1,3-divinyl-1,1,3,3-tetramethyldisiloxane platinum(II) complex was purchased by Gelest ABCR GmbH Co. (Karlsruhe, Germany). Nickel acetate tetrahydrate [Ni(Ac)₂·4H₂O], supplied by Vetec Química Fina Ltda (Rio de Janeiro, Brazil), was previously dried (NiAc) and toluene P.A. was supplied by Synth (Diadema, Brazil).

Synthesis of the siloxane-clay composite

Initially, NiAc was incorporated into PDMS-PEO²¹ followed by the MT addition. The resulting mixture was blended in a MARCONI mechanical stirrer at 1000 rpm during 2 h. This mixture was added to a solution of PMS and DVB, catalyzed by Pt(II) complex, which was in 1:1 ratio, considering the molar relation of Si-H bonds (from PMS) and C=C bonds (from DVB) and then mixed according to the procedure previously described,⁴ to

give rise to the polymeric matrix of the composite. The final mixture was blended until a viscous solution was obtained, which was immediately poured into a steel mold of $(13.5 \times 1.3 \times 0.3) \text{ cm}^3$. The final content of PDMS-PEO, MT and NiAc was 18, 36 and 1 wt.%, respectively. The obtained material was cured at 80 °C and ca. 80 MPa for 1 h in a MARCONI molding machine, in the absence of inert atmosphere. The final product, named green body (GB), was additionally cured at 100 °C in a vacuum oven for 8 h.

Ceramic materials preparation

The ceramic materials (CM) were obtained by controlled pyrolysis of the GB at 950 °C (CM950), followed by heat treatment at 1500 °C (CM1500), at a heating rate of 5 °C min⁻¹ and a holding time of 60 min at the final selected temperature. The pyrolyses were carried out in EDG 5P tubular furnace, equipped with an internal alumina tube and a temperature controller, under argon flow (100 mL min⁻¹), using a multi-step-heating schedule. For the sample obtained at 1500 °C, the heat treatment procedure was carried out from a sample previously pyrolysed at 950 °C in a Thermolyne F59340-CM tubular furnace.

Characterization techniques

Thermal stability and ceramic yield of the green body were analysed by thermogravimetry (TG) in a TA 2950 thermobalance (TA Instruments, New Castle, DE) from 25 to 980 °C, at a heating rate of 20 °C min⁻¹ under argon flow (100 mL min⁻¹).

The structural evolution from the siloxane-clay composites to ceramic materials was monitored by infrared (IR) spectroscopy, using a Bomem B100 spectrometer, operating in the transmission mode between 4000 and 400 cm⁻¹, at 4 cm⁻¹ resolution.

X-ray diffraction (XRD) patterns were recorded on a Shimadzu diffractometer, model XRD6000, using Cu K α radiation ($\lambda = 1.54060 \text{ \AA}$).

Micro-Raman scattering was obtained in a Renishaw Raman microscope with excitation by an Ar laser (514.5 nm), potency of 1.1 mW cm⁻² and calibration of the Si peak at 520.7 cm⁻¹. The error in the peak positions was less than $\pm 2.0 \text{ cm}^{-1}$.

Micro-, meso- and macroporosities were evaluated by both nitrogen adsorption/desorption and mercury intrusion porosimetry techniques. The specific surface area, total pore volume and average pore size were obtained from N₂ adsorption experiments, on a fully automatic nitrogen gas adsorption apparatus (Autosorb, Quantachrome Instruments), which can be programmed to measure gas

adsorption and desorption isotherms. The surface area was obtained from the N₂ adsorption isotherms by using the Brunauer, Emmet and Teller (BET) method.²⁴ The total pore volume was calculated by using the N₂ desorption isotherm, following the Barret, Joyner and Halenda (BJH) method.²⁵ In order to full comprises the porosity features of the samples, open porosity was characterized by high-pressure mercury intrusion (PoreMaster, Quantachrome), with intrusion pressures from 20 to 33000 psi. Pore size distributions were calculated from the intrusion curve by using the Washburn equation.²⁶ A value of 140° was used for the contact angle of the mercury on the solid, and the surface tension of the mercury was taken at 480 erg cm⁻². The samples were outgassed up to 50 mmHg immediately prior to analysis to facilitate the filling of the penetrometers with mercury.

Density measurements were performed in a helium pycnometer (Micromeritics, model 1305), using helium as carrier gas. The analyses were conducted with samples dried at 120 °C for 1 h and purged with helium at least 10 times before measuring. These measurements correspond to bulk density and the obtained values include the closed pores.

The morphology of fracture surface of the samples was observed by scanning electron microscopy (SEM) using a JEOL JSM 6360-LV microscope with an accelerating voltage of 20 keV. Previously to analyses, the exposed fracture surface was covered with a thin layer of Au/Pd alloy, using a Bal-Tec MED 020 equipment. The chemical composition analysis of Si, O and C elements was performed by energy dispersive spectroscopy (EDS) technique.

Results and Discussion

Thermal stability of the MT, MT/PDMS-PEO and GB

The TG and DTG curves for MT, MT/PDMS-PEO and GB are illustrated in Figure 1.

The MT presented two main steps of weight loss: the first (28-184 °C), with a loss of 2.7%, can be attributed to the presence of weakly bonded water and intercalated water into the interlayer regions, and the second stage (460-750 °C), which corresponds to a weight loss of 5%, is related to the loss of structural hydroxyl groups.^{27,28} The curves for MT/PDMS-PEO showed the thermal decomposition of PDMS-PEO, with a weight loss of 47% (220-550 °C), and also the steps observed for MT. The first weight loss of GB, from ca. 80 to 350 °C (4.3%), corresponded to volatile monomer not included in the polymeric network. A weight loss of 15% (440-640 °C) was

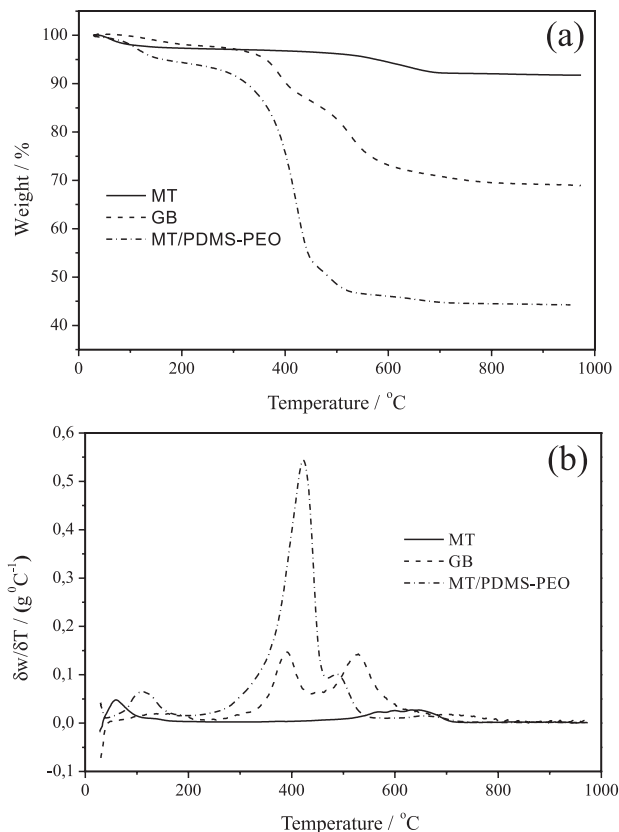


Figure 1. TG and DTG curves: MT, MT/PDMS-PEO and GB.

attributed to the degradation of organic groups, involving C–H, C–C and Si–C bond scissions of Si–CH₃ and Si–CH₂–CH₂ residual groups.²⁹ From 640 °C to 840 °C, part of the phenyl rings can be degraded, followed by the formation of inorganic material.³⁰ In this last step, reorganization reactions of Si sites can also take place, giving rise to silicon oxycarbide formation. At 980 °C, the ceramic yield obtained for GB was 69%.

Structural characterization from green body to the ceramic materials

The structural evolution from GB to the ceramic materials (CM950 and CM1500) was monitored by IR analyses and the spectra are showed in Figure 2.

In the GB spectrum, a drastic reduction of ν C=C (ca. 3055 cm⁻¹) and ν Si–H (ca. 2162 cm⁻¹) absorptions³¹ were observed, compared to DVB and PMS pristine spectra, respectively. This result indicated that the hydrosilylation reaction between PMS and DVB was effective, generating a hybrid polymeric network. For the sample pyrolyzed at 950 °C, CM950, the disappearance of the absorption bands from 2966 to 2869 cm⁻¹ of the CH₃ and CH₂ groups was verified, indicating the formation of a typical inorganic material. A recent study showed that the conversion process

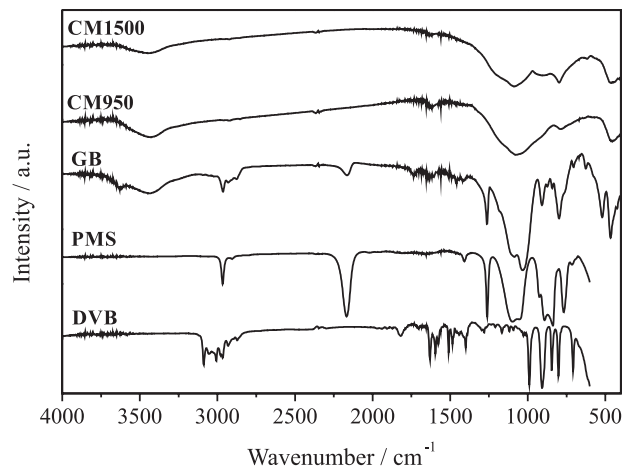
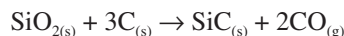


Figure 2. IR spectra of PMS, DVB and GB starting materials and CM950 and CM1500 ceramic materials.

from PMS/DVB polymeric network to ceramic material is already practically complete at 700 °C.⁴ The broad bands at ca. 1080 and 800 cm⁻¹ are assigned to ν Si–O–Si and ν Si–C absorptions, respectively, as expected for the CM950. The relative intensity and width of the absorption centered at 1080 cm⁻¹ (ν Si–O–Si) decreased with increasing of the temperature from 950 to 1500 °C, as showed in the CM950 and CM1500 spectra. In addition, an increase in the relative intensity of the absorption at 800 cm⁻¹ (ν Si–C) was observed. These results indicated that at high heat treatment temperature, the formation of silicon carbide (SiC) is more intense. This behavior is expected, once it is well established that SiC is formed at temperatures higher than 1300 °C by a carbothermal reduction reaction of Si–O and C rich sites present in a non-crystalline SiC_xO_y phase,^{32,33} as illustrated by reaction scheme below:



The IR spectra for CM950 and CM1500 samples also showed the presence of a weak absorption at 480 cm⁻¹, characteristic of ν Si–O, which corresponds to the mode associated with cyclic siloxane.

The XRD patterns for GB and CM950 and CM1500 ceramic materials are showed in Figure 3.

The GB showed a single (001) diffraction peak at $2\theta = 5.5^\circ$, corresponding to the MT d-spacing (interlayer distance) of 1.60 nm, calculated according to Bragg's equation. The d-spacing of MT is higher than that of the pristine montmorillonite (1.26 nm, not shown) due to the insertion of PDMS-PEO between clay galleries. Other diffraction peaks, with characteristic intensities at 20°, 35° and 62° (2θ), corresponding to (100), (110) and (060) smectite plane reflections,³⁴ respectively, were also observed.

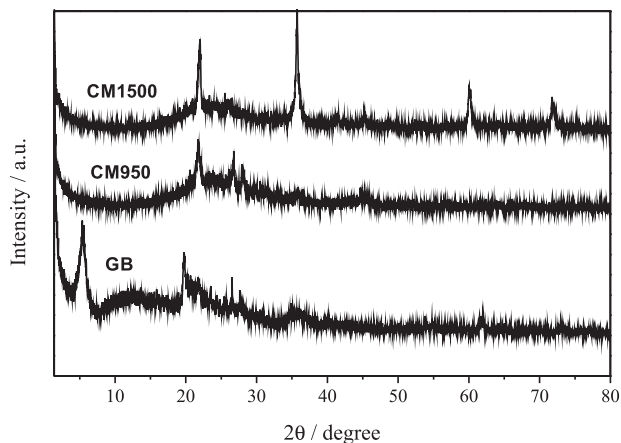


Figure 3. X-ray diffraction patterns of GB, CM950 and CM1500 ceramic materials.

During the conversion process from polymeric precursor to ceramic, the layered structure of the MT is destroyed and the clay (001) diffraction peak is not more observed in the ceramic materials. XRD pattern for CM950 showed the formation of cristobalite silica ($c\text{-SiO}_2$) at 22° and 28° (2θ),³⁵ C-graphite at 26.1° (2θ), attributed to its (002) plane,³⁶ and lower intensity reflections at 35.5° and 45.4° (2θ), corresponding to (111) plane³⁷ of $\beta\text{-SiC}$ and Ni_2Si phases,³⁰ respectively. These reflections became more intense with increasing of the temperature, as can be observed in the XRD pattern for CM1500 sample. Moreover, additional peaks of the characteristic $\beta\text{-SiC}$ phase at 60° and 72° (2θ) were also verified for CM1500, related to the (220) and (311) planes,³² confirming the more effective crystallization of the $\beta\text{-SiC}$ phase for sample obtained at 1500°C , as also showed in the IR spectra. The peak at 42° (2θ) was assignment to Ni_3C phase,^{38,39} probably formed during methane and hydrogen gases released in the pyrolysis process. Apart from the increasing of the temperature has favoured the formation of crystalline phases in a SiC_xO_y matrix, the presence of Ni was crucial to this process. Recently, studies about structural evolution from PMS/DVB hybrid networks to ceramic materials, with emphasis to the Ni addition in the polymeric precursors, were performed. The results stated that Ni acted as an inductor of the crystallization process, reducing the activation energy towards the $c\text{-SiO}_2$, $\beta\text{-SiC}$ and graphitic carbon phases, in comparison with the material without Ni obtained at the same temperature.⁴ Thus, in the present study, the presence of NiAc in the polymeric precursor certainly contributed to an effective crystallization of the resulting ceramics, according to previously results.⁴

Polysiloxanes-derived ceramics generally contains an excess of carbon in its structure, known as dispersed carbon phase (C_{free}) (secondary phase), where the carbon atoms were not bonded to the polymeric network. The presence

of the C_{free} in the ceramic matrices was evaluated by Raman spectroscopy, which is a technique usually employed for the characterization of C-containing materials. Figure 4 displays the Raman spectra for CM950 and CM1500 samples.

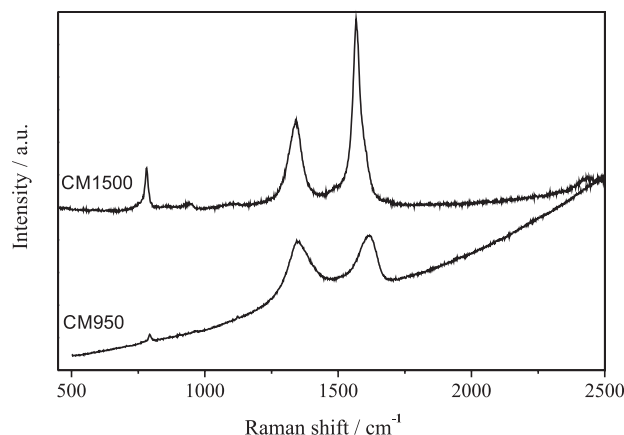


Figure 4. Raman spectra of CM950 and CM1500 ceramic materials.

The spectra for both materials showed two typical features of disordered graphitic forms: the D (disordered) band at ca. 1350 cm^{-1} and the G (graphite) band at around 1600 cm^{-1} .⁴⁰⁻⁴² The spectral profile for CM950 showed a less intense band at 791 cm^{-1} , characteristic of SiC phase,⁴³ whereas for CM1500 this band became more intense, in addition to the presence of a less intense band at 944 cm^{-1} , which also corresponds to SiC phase. The identification and behavior of the SiC phase by Raman spectra, considering the increase of the temperature, is in agreement with IR and XRD data. As can be clearly verified, CM950 spectrum exhibited a large fluorescence background, mainly above 2000 cm^{-1} , characteristic of these non-crystalline materials,⁴⁴ with broader D- and G-bands. It has been reported that the pronounced fluorescence phenomenon can prevent the identification of the C_{free} phase, as verified in C-rich SiCO ceramics heated at 1400°C .^{33,45} According to these authors, this phenomenon may be associated with defects present in the samples and radical formation during the polymer-to-glass transformation.

The increase of the temperature from 950 to 1500°C promoted a decrease in the fluorescence background. In addition, the valley between D- and G-bands became deeper, with smaller full width half-maxima (FWHM). CM950 sample revealed a value of 195 cm^{-1} for D-band, while for CM1500 this value was 61 cm^{-1} . This result indicates that at 1500°C , the ceramic sample exhibited very distinct D- and G-bands, characterized by rather narrow peaks, which suggests that an ordering process occurred within the C_{free} phase during heat treatment of these samples, confirmed

by smaller FWHM value of D-band for CM1500 sample. The typical increase in the intensity of the G band and concomitant decrease of the D band is indicative that turbostratic carbon was formed at 1500 °C.⁴⁶ Moreover, D-and G-bands slightly shifted for lower frequencies values with increasing of pyrolysis temperature. This behavior for D-band suggests a decrease in a number of ordered aromatic rings on passing from nano-crystalline graphite to non-ordered carbon structure.⁴¹ The G-band position in graphite carbon-containing materials, however, is expressed according to amount of Csp³ sites, in which increasing the amount of these carbon sites shifts G-band to lower values, just verified for CM1500.

Porosity measurements

Initially, ceramic materials were submitted to the N₂ adsorption technique (isotherms not showed) in order to characterize the micro- and mesopores, followed by the high-pressure Hg intrusion to supply a complete porosity characterization, once this last technique evaluates the meso- and macropores range in these materials. Table 1 shows specific surface area, total pore volume, average pore size, porosity and bulk density values, obtained by N₂ adsorption, Hg intrusion porosimetry and density measurements, of the ceramic materials produced at 950 °C and 1500 °C. As observed, the low specific surface area value provides a prediction that polymer-derived ceramics are classified as dense materials, revealing extremely low values, in the 1-2 m² g⁻¹ range.⁴⁷ The specific surface area values, determined by the BET method, showed tendency to increase with increasing of the temperature, as well as the total pore volume values obtained by BJH method. This behavior is attributed to the intense carbothermal reduction reaction at 1500 °C, as result of the reorganization reactions of different silicon sites, promoting the β-SiC phase crystallization and thus the reduction of the SiO₂ and C phases from ceramic matrix. This phenomenon probably contributed to the increase in the porosity (Hg intrusion porosimetry) from 19.2 to 28.3 % of the ceramic materials obtained at 950 °C and 1500 °C, respectively, which is in agreement to SEM

illustrations exhibited in the next section. Additionally, the average pore size of CM950 and CM1500 samples (1.5 and 1.9 nm, respectively) confirmed that both materials presented microporous into ceramic matrix, which are in the considered range for this classification ($d < 2$ nm).⁴⁸ Then, as earlier described, the N₂ adsorption/desorption technique detects the micro- and mesopores range, however, in these ceramic materials, only the presence of micropores was verified.

The effect promoted by the temperature on the crystallization of the resulting ceramics generally gives rise to changes in the density of the resulting materials. It is well known that SiC_xO_y glasses derived from polymeric precursors present a glass transition temperature in the 1300-1350 °C range.⁴⁹ Thus, above the glass transition temperature of the SiC_xO_y glass, the densification of the specimens takes place as a consequence of a viscous sintering process. In addition, the carbothermal reduction reaction also contributes to the formation of the β-SiC crystalline phase (density of 3.21 g cm⁻³)⁵⁰ and, consequently, to the increase of the density value. Although CM1500 reveals higher crystallinity than CM950 sample, comprised by the intense and well-defined diffraction peaks, its density value was slightly lower. This behavior may be explained by higher average pore size and porosity values for CM1500 when compared with the CM950 sample.

High-pressure Hg porosimetry is a widely employed technique for evaluating of the open-porosity and pore size distribution in ceramic materials. This technique comprises the mesopores (2 < d < 50 nm) and macropores (d > 50 nm) range, limiting only for micropores range (d < 2 nm).⁴⁸ The equipment possesses two analysis stations: the low pressure station (from 0 to 50 psi), which determines pores with higher diameters and the high pressure station (from 0 to 33000 psi), which comprises the region of pores with lower sizes present in the material. After analyzing, it is generated a standard curve of the Hg intruded volume in function of the pressure necessary for the penetration of Hg inside pores. Figure 5 illustrates the histograms of normalized volume (Hg intruded volume in relation to sample mass ratio) as a function of pore diameter for CM950 and CM1500 obtained by Hg intrusion technique.

Table 1. Specific surface area, total pore volume, average pore size, porosity and bulk density values of the CM950 and CM1500 ceramic materials, obtained by N₂ adsorption, Hg intrusion porosimetry and density measurements

Ceramic materials	Specific surface area ^a / (m ² g ⁻¹)	Total pore volume ^a / (10 ⁻³ cm ³ g ⁻¹)	Average pore size ^a / nm	Porosity ^b / %	Bulk density ^c / (g cm ⁻³)
CM950	0.5	1.7	1.5	19.2	1.0
CM1500	2.0	9.6	1.9	28.3	0.9

^aData obtained from N₂ adsorption isotherms; ^bdata obtained from Hg intrusion porosimetry; ^cvalue obtained in a helium pycnometer using helium as carrier gas.

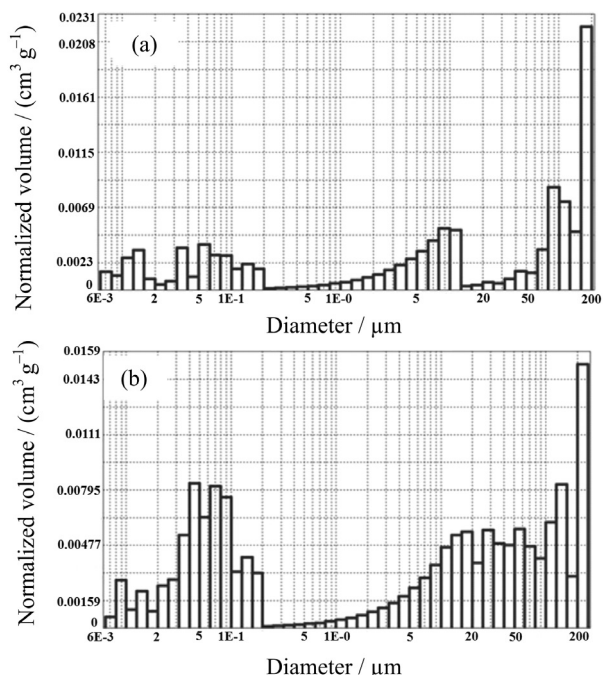


Figure 5. Normalized volume as a function of diameter of CM950 (a) and CM1500 (b) samples obtained from mercury porosimetry technique.

Both samples showed wide pore size distribution, in the meso- and macropores regions. As observed, CM1500 revealed higher amount of mesopores than CM950, mainly for those with sizes between 35 and 50 nm (initial left part of histogram). In addition, a more significant amount of macropores with diameters lower than 100 μm was also verified for ceramic obtained at 1500 °C. However, CM950 showed a more pronounced macroporosity than CM1500 for pores with sizes higher than 100 μm, mainly for sizes around 200 μm (final right part of histogram). The presence of the generated pores can be clearly seen in the SEM images (next section), where the wide range of sizes is comparable to porosity results, mainly related to macropores. In this way, high-pressure Hg porosimetry allowed a complete porosity characterization for studied ceramics, revealing the presence of meso- and macropores in both materials, where these last are not possible to be identified by the N₂ adsorption/desorption technique.

Morphological evaluation

Figure 6 shows that the fracture surface morphology of the CM950 is mainly formed by islands with different sizes and shapes together with high amount of polydisperse pores associated to the PDMS-PEO degradation. As can be seen in the magnified area of Figure 6a, the islands are distributed all over the surface of the sample as well as inside the pores (Figure 6b).

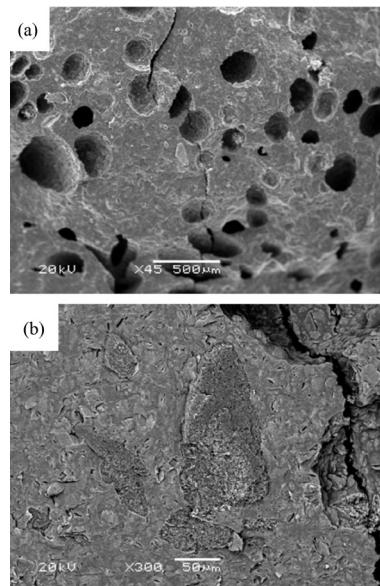


Figure 6. SEM micrographs of CM950.

SEM observations coupled with EDS analysis revealed that the islands are basically composed by carbon and nickel elements, as illustrated in Figure 7. The presence of these elements suggests the formation of the nickel carbide (Ni₃C) phase which is rather unusual carbide, once this phase is not stable at high temperature.³⁹ Probably, this phase was produced in small amount in the ceramic matrix. The Ni₃C generated in CM950 was only verified by SEM-EDS; however, it was not identified by XRD, since it is not sufficiently sensitive to detect a small amount of this phase. Nickel carbide is usually prepared by the reaction of some activated form of nickel metal with carbon monoxide.⁵¹ The formation of the carbide phase can occur via adsorption of a C-containing matrix constituent on the surface of a nickel cluster and subsequent decomposition of the absorbed molecule, whereas the carbon diffuses into the nickel to form the carbide phase.⁵² Kashiwagi *et al.*⁵³ used sucrose as a carbon source to synthesize Ni₃C nano-whiskers, by means of the spray pyrolysis technique at 800 °C. Podsiadly *et al.*³⁹ reported the effective synthesis of nanocrystalline nickel and iron carbides through hydrocarbons decomposition on respective metal catalysts at different temperatures. In the present study, however, the main carbon sources are the DVB component from the hybrid polymeric network precursor, which, under inert argon atmosphere, generates dispersed C_{free} from incomplete thermal degradation of aliphatic and aromatic groups of the organic specie, and volatile hydrocarbons such as hydrogen and methane released during pyrolysis process.

Figure 8 shows the fracture surface morphology of the CM1500. The morphological investigation of the ceramics supported the porosity data.

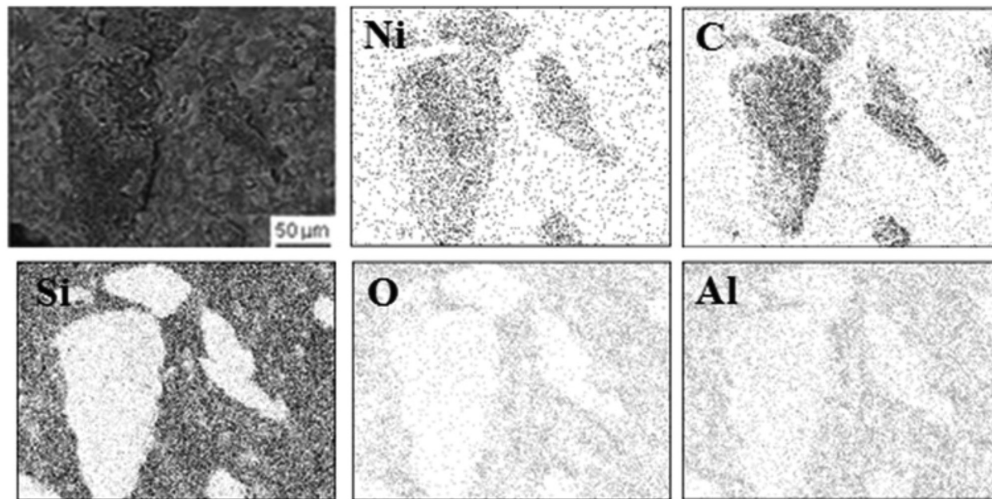


Figure 7. SEM/EDS micrograph and Ni, C, Si, O and Al elemental maps of CM950.

CM1500 presented a higher amount of pores (Figure 8a) than CM950 (Figure 6a), which can be associated to the reorganization reactions of different silicon sites, as explained for the porosity data, besides the effective PDMS-PEO degradation. An important feature related to the morphology of the CM1500 was the presence of ultra-long nanowires formed in some pores, as shown in Figures 8b and 8c (Figure 8c corresponds to amplified region from Figure 8b). These nanowires of large aspect ratio are normally entangled and randomly oriented, similar to typical carbon nanotubes morphology.^{39,54} EDS analysis (not shown) revealed that the nanowires are probably composed by carbon, oxygen and silicon elements (32, 33 and 15 wt.% respectively). However, this will be further investigated. The Ni- and C-rich islands of the CM950, associated to presence of pores, probably contributed to the formation of the nanowires at higher temperature (1500 °C). Podsiadly *et al.*³⁹ reported that carbon nanostructures (nanotubes and/or nanofibers) can be produced through the decomposition of the metal carbides, preferentially on metals able to form unstable carbides. The authors observed that the formation of catalytic nickel carbide phase was associated to chemical composition of hydrocarbons in the reaction medium and decomposition temperature. Hydrocarbons containing high amounts of hydrogen in relation to carbon atoms led to reduction of this carbide phase, whereas smaller hydrogen to carbon ratios exhibited opposite behavior. In this way, the small amount of Ni₃C obtained in this study could be justified by relatively hydrogen-rich atmosphere, generated by thermal decomposition of Si-CH₃ and Si-H bonds from polymeric network and pyrolysis temperatures, since Ni₃C decomposition is usually more favored than its formation at high temperatures.³⁹ Moreover, it can be accepted that the pores, specifically, can provide enough growth space

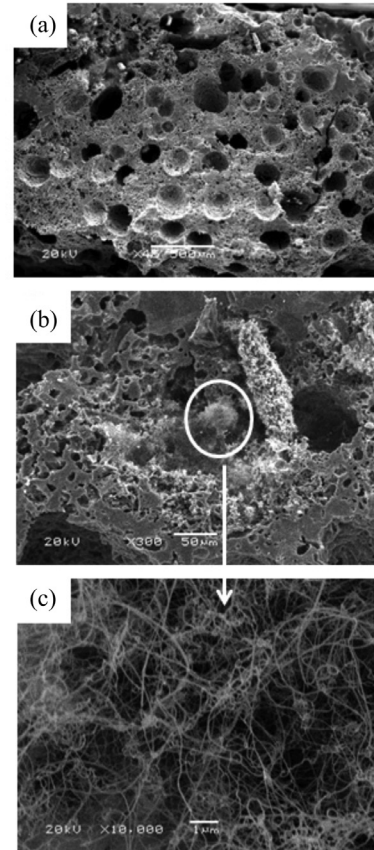


Figure 8. SEM micrographs of CM1500.

for nanowires.⁵⁵ The presence of NiAc in the polymeric precursor has been reported to be effective for inducing nanowire formation with different morphologies in the ceramic products when compared to ceramics prepared without Ni.²² The formation of these typical nanostructures in the polymer-derived ceramics, generally promoted by specific techniques using or not transition metals, becomes

these materials with potential applications for catalyst support⁵⁶ and those related to construction of nanoscale electronic and optoelectronic devices.⁵⁷

Conclusions

In summary, this study describes the effect of the Ni and the pyrolysis temperature on the structural, textural and morphological features of SiCO-derived ceramic, obtained from polysiloxane-clay composites, in the presence, or not of Ni. The carbothermal reduction reaction occurred at temperature above 1200 °C and, mainly, in the presence of NiAc in the polymeric precursor. From 950 °C to 1500 °C, the C_{free} phase, typical of SiCO-derived ceramics, exhibited an ordering process, as verified by Raman spectra. Complementary porosity techniques showed the wide pore size distribution, comprising pores in the micro, meso and macro scales. However, the results indicated that CM1500 possesses higher pore amounts, justifying the formation of nanowires only in this sample. The presence of Ni metal was crucial to effective production of the nanowires in some areas of the ceramic products, making them as a candidate material in future applications, such as optoelectronic devices and catalyst support.

Acknowledgements

We gratefully acknowledge financial support from FAPESP (Fundação de Amparo à Pesquisa do Estado de São Paulo) (Processes 05/58460-0 and 03/09926-1) and CNPq (Conselho Nacional de Desenvolvimento Científico e Tecnológico) (Proc. 305916/2006-8). The authors also thank Alfredo Tiburcio Nunes Pires for Raman measurements.

References

- Duan, L.; Ma, Q.; *Ceram. Int.* **2012**, *38*, 518.
- Tamayo, A.; Rubio, J.; Rubio, F.; Oteo, J. L.; Riedel, R.; *J. Eur. Ceram. Soc.* **2011**, *31*, 1791.
- Dong, S.; Li, Y. L.; An, H. J.; Liu, X.; Hou, F.; Li, J. Y.; Fu, X.; *J. Eur. Ceram. Soc.* **2010**, *30*, 1503.
- Segatelli, M. G.; Pires, A. T. N.; Yoshida, I. V. P.; *J. Eur. Ceram. Soc.* **2008**, *28*, 2247.
- Schiavon, M. A.; Ciuffi, K. J.; Yoshida, I. V. P.; *J. Non-Cryst. Solids* **2007**, *353*, 2280.
- Tian, H.; Ma, Q. S.; Pan, Y.; Liu, W. D.; *Ceram. Int.* **2013**, *39*, 71.
- Kim, B. S.; Kim, D. J.; *J. Eur. Ceram. Soc.* **2007**, *27*, 837.
- Greil, P.; *J. Am. Ceram. Soc.* **1995**, *8*, 835.
- Siqueira, E. J.; Yoshida, I. V. P.; Pardini, L. C.; Schiavon, M. A.; *Ceram. Int.* **2009**, *35*, 213.
- Martin, T.; Galarneau, A.; DiRenzo, F.; Brunel, D.; Fajula, F.; Heinisch, S.; Crétier, G.; Rocca, J. L.; *Chem. Mater.* **2004**, *16*, 1725.
- Hojamberdiev, M.; Prasad, R. M.; Morita, K.; Zhu, Y.; Schiavon, M. A.; Gurlo, A.; Riedel, R.; *Appl. Catal. B* **2012**, *115-116*, 303.
- Seo, D.; Jung, S.; Lombardo, S. J.; Feng, Z. C.; Chen, J. K.; Zhang, Y.; *Sens. Actuators A* **2011**, *165*, 250.
- Vakifahmetoglu, C.; Presser, V.; Yeon, S. H.; Colombo, P.; Gogotsi, Y.; *Microporous Mesoporous Mater.* **2011**, *144*, 105.
- Chae, S. H.; Kim, Y. W.; Song, I. H.; Kim, H. D.; Narisawa, M.; *J. Eur. Ceram. Soc.* **2009**, *29*, 2867.
- Hojamberdiev, M.; Prasad, R. M.; Morita, K.; Schiavon, M. A.; Riedel, R.; *Microporous Mesoporous Mater.* **2012**, *151*, 330.
- Colombo, P.; *J. Eur. Ceram. Soc.* **2008**, *28*, 1389.
- Malenfant, P. R. L.; Wan, J.; Taylor, S. T.; Manoharan, M.; *Nat. Nanotechnol.* **2007**, *2*, 43.
- Krawiec, P.; Geiger, D.; Kaskel, S.; *Chem. Commun.* **2006**, *23*, 2469.
- Nghiem, Q. D.; Kim, D.; Kim, D. P.; *Adv. Mater.* **2007**, *19*, 2351.
- Majoulet, O.; Alauzun, J. G.; Gottardo, L.; Gervais, C.; Schuster, M. E.; Bernard, S.; Miele, P.; *Microporous Mesoporous Mater.* **2011**, *140*, 40.
- Kaneko, M. L. Q. A.; Torriani, I. L.; Yoshida, I. V. P.; *J. Braz. Chem. Soc.* **2007**, *18*, 765.
- Segatelli, M. G.; Radovanovic, E.; Gonçalves, M. C.; Yoshida, I. V. P.; *J. Eur. Ceram. Soc.* **2009**, *29*, 3279.
- Li, F.; Wen, G.; Song, L.; *J. Cryst. Growth* **2006**, *290*, 466.
- Brunauer, S.; Emmett, P. H.; Teller, E.; *J. Am. Chem. Soc.* **1938**, *60*, 309.
- Barrett, E. P.; Joyner, L. G.; Halenda, P. P.; *J. Am. Chem. Soc.* **1951**, *73*, 373.
- Webb, P. A.; Orr, C.; *Analytical Methods in Fine Particle Technology*, Micromeritics Instrument Corp.: Norcross, 1997.
- Guggenheim, S.; Koster van Groos, A. F.; *Clays Clay Miner.* **2001**, *49*, 433.
- Le Pluart, L.; Duchet, J.; Sautereau, H.; Gérard, J. F.; *J. Adhes.* **2002**, *78*, 645.
- Michalczyk, M. J.; Farneth, W. E.; Vega, A. J.; *Chem. Mater.* **1993**, *5*, 1687.
- Scheffler, M.; Greil, P.; Berger, A.; Pippel, E.; Woltersdorf, J.; *Mater. Chem. Phys.* **2004**, *84*, 131.
- Bellamy, L. J.; *The Infra-Red Spectra of Complex Molecules*, 2nd ed.; John Wiley & Sons: London, 1958.
- Schiavon, M. A.; Radovanovic, E.; Yoshida, I. V. P.; *Powder Technol.* **2002**, *123*, 232.
- Alonso, R. P.; Mariotto, G.; Gervais, C.; Babonneau, F.; Sorarù, G. D.; *Chem. Mater.* **2007**, *19*, 5694.
- Venaruzzo, J. L.; Volzone, C.; Rueda, M. L.; Ortiga, J.; *Microporous Mesoporous Mater.* **2002**, *56*, 73.
- Bois, L.; Maquet, J.; Babonneau, F.; *Chem. Mater.* **1995**, *7*, 975.

36. Cheng, J.; Zhang, X.; Ye, Y.; *J. Solid State Chem.* **2006**, *179*, 91.
37. JCPDS File 29 1129.
38. Fujieda, S.; Shinoda, K.; Suzuki, S.; Jeyadevan, B.; *Mater. Trans.* **2012**, *53*, 1716
39. Podsiadly, M.; Pelech, I.; Narkiewicz, U.; *Mater. Sci.-Poland.* **2013**, *31*, 65
40. Tuinstra, F.; Koenig, J. L.; *J. Chem. Phys.* **1970**, *53*, 1126.
41. Ferrari, A. C.; Robertson, J.; *Phys. Rev. B* **2000**, *61*, 14095.
42. Yan, M.; Song, W.; Zhao-hui, C.; *Ceram. Int.* **2010**, *36*, 2455.
43. Trassl, S.; Motz, G.; Rössler, E.; Ziegler, G.; *J. Non-Cryst. Solids* **2001**, *295*, 261.
44. Kleebe, H. J.; Gregori, G.; Babonneau, F.; Blum, Y. D.; MacQueen, D. B.; Masse, S.; *Int. J. Mater. Res.* **2006**, *97*, 699.
45. Bréquel, H.; Parmentier, J.; Walter, S.; Badheka, R.; Trimmel, G.; Masse, L. J.; Dempsey, P.; Turquat, C.; Desmartin-Chomel, A.; Le Neindre-Prum, A. L.; Jayasooriya, U. A.; Hourlier, D.; Kleebe, H. J.; Sorarù, G. D.; Enzo, F.; Babonneau, G. F.; *Chem. Mater.* **2004**, *16*, 2585.
46. Graczyk-Zajac, M.; Mera, G.; Kaspar, J.; Riedel, R. J. *Eur. Ceram. Soc.* **2010**, *30*, 3235.
47. Kleebe, H. J.; Gregori, G.; Babonneau, G. F.; Blum, Y. D.; MacQueen, D. B.; Masse, S.; *Int. J. Mater. Res.* **2006**, *97*, 699.
48. Lowell, S.; Shields, J. E.; Thomas, M. A.; Thommes, M.; *Characterization of Porous Solids and Powders: Surface Area, Pore Size and Density*, 2nd ed.; Springer: Netherlands, 2006.
49. Rouxel, T.; Massouras, G.; Sorarù, G. D.; *J. Sol-Gel Sci. Technol.* **1999**, *14*, 87.
50. Yang, H.; Zhao, H.; Li, Z.; Zhang, K.; Liu, X.; Tang, C.; *Ceram. Int.* **2012**, *38*, 2213.
51. Hooker, P.; Tan, B. J.; Klabundle, K. J.; Suib, S.; *Chem. Mater.* **1991**, *3*, 947.
52. Bonder, M. J.; Kirkpatrick, E. M.; Martin, T.; Kim, S. J.; Rieke, R. D.; Pelecky, D. L. L.; *J. Magn. Magn. Mater.* **2000**, *222*, 70.
53. Kashiwagi, T.; Suzuki, N.; Niina, M.; Nishiguchi, H.; Nagaoka, K.; Takita, Y.; *Chem. Lett.* **2007**, *36*, 512.
54. Menzer, K.; Krause, B.; Boldt, R.; Kretzschmar, B.; Weidisch, R.; Pötschke, P.; *Composites Sci. Technol.* **2011**, *71*, 1936.
55. Pan, J.; Yan, X.; Cheng, X.; Lu, Q.; Wang, M.; Zhang, C.; *Ceram. Int.* **2012**, *38*, 6823.
56. Lee, J. S.; Lee, S. H.; Choi, S. C.; *J. Alloys Compd.* **2009**, *467*, 543.
57. Li, G.; Wen, G.; Song, L.; *J. Cryst. Growth* **2006**, *290*, 466.

Submitted on: October 18, 2013

Published online: February 4, 2014

FAPESP has sponsored the publication of this article.